LAWRENCE
LIVERMORE
NATIONAL
LABORATORY

LLNL-TR-405903

Progress in model development to quantify High Explosive Violent Response (HEVR) to mechancial insult

J. E. Reaugh

August 1, 2008

Disclaimer

This work performed under the auspices of the U.S. Department of Energy by Lawrence Livermore National Laboratory under Contract DE-AC52-07NA27344.

Progress in model development to quantify High Explosive Violent Response (HEVR) to mechanical insult

John E. Reaugh

1. Introduction

The rapid release of chemical energy has found application for industrial and military purposes since the invention of gunpowder. Black powder, smokeless powder of various compositions, and pyrotechnics all exhibit the rapid release of energy without detonation when they are being used as designed. The rapidity of energy release for these materials is controlled by adjustments to the particle surface area (propellant grain configuration or powder particle size) in conjunction with the measured pressure-dependent burning rate, which is very subsonic. In this way a manufacturing process can be used to engineer the desired violence of the explosion. Detonations in molecular explosives, in contrast, propagate with a supersonic velocity that depends on the loading density, but is independent of the surface area. In ideal detonations, the reaction is complete within a small distance of the propagating shock front. Non-ideal detonations in molecular and composite explosives proceed with a slower velocity, and the reaction may continue well behind the shock front.

We are developing models to describe the circumstances when molecular and composite explosives undergo a rapid release of energy without detonating. The models also apply to the behavior of rocket propellants subject to mechanical insult, whether for accidents (Hazards) or the suite of standardized tests used to assess whether the system can be designated an Insensitive Munition (IM). In the application described here, we are studying an HMX (1,3,5,7-tetranitro-1,3,5,7-tetraazacyclooctane) explosive developed in the UK, which is 91% by weight HMX and 9% binder-plasticizer. Most explosives and propellants, when subjected to a mechanical insult, drop or impact that is well below the threshold for detonation have been observed to react violently. This behavior is known as High Explosive Violent Reaction (HEVR). The basis of our model is the observation that the mechanical insult produces damage in a volume of the explosive near the trajectory of the impactor. The damage is manifest as surface area through the creation of cracks and fragments, and also as porosity through the separation of crack faces and isolation of the fragments. Open porosity permits a flame to spread easily and so ignite the surface area that was created. The surface area itself leads to in increase in the mass-burning rate. As the kinetic energy and power of the insult increases, the degree of damage and the volume of damage both increase. Upon a localized ignition, the flame spreads to envelop the damaged volume, and the pressure rises at an accelerated rate until neither mechanical strength nor inertial confinement can successfully contain the pressure. The confining structure begins to expand. This reduces the pressure and may even extinguish the flame. Both the mass of explosive involved and the rate at which the gas is produced contribute to each of several different measures of violence. Such measures include damage to the confinement, the velocity and fragment size distributions from what was the confinement,

and air blast. Figure 1 illustrates the interaction of the various phenomena described above.

Our model comprises several interacting elements. The production of damage, the ignition criterion, the mass rate of burning (reaction rate), the equations of state and constitutive models of the solid explosive reactant (unburned) and gas products, flame propagation in damaged reactant, and the progressive failure of the confinement are all elements of the model. The model is intended for implementation in a general-purpose simulation program (hydrocode) that solves the partial differential equations for the conservation of mass, momentum, and energy in conjunction with equations of state and strength.

2. HE damage in response to mechanical insult

Both rocket propellants and high-performance explosives are composite materials. They are formed of independent granules with broad bimodal or trimodal particle size distributions to achieve a high packing density of solids. They are held together with a polymeric plastic binder, typically less than 15% by volume, and either nil void volume (for solid rocket propellants and the UK explosive we are studying) or 2 to 5% void volume. As a result, the mechanical response has features in common with rocks and soils, which are granular materials, and also the rate dependence exhibited by other filled polymers.

Constitutive models developed for rocks and soils incorporate the pressure dependence of shear strength and the increase in volume during fracture and continued shearing of broken material. The models typically do not quantify the increase in surface area. For our needs, the surface area is an important element in the response because the mass-burning rate is directly dependent on surface area. Constitutive models developed for filled polymers exhibit rate dependence and the interplay of ambient temperature with strain rate, but typically do not address the post failure shear or the pressure dependence.

2.1 Model for surface area

Results from a standardized test of propellants and explosives called the friability test in the UK and the shotgun test in the US provided data with which we calibrated a model for surface area. In that test, right circular cylinders of the subject material are formed, and a sequence of Taylor impact tests [1, 2] is performed at various velocities in the typical range of 100 to 400 m/s. At a US Navy laboratory (China Lake) and elsewhere, the cylinders are launched from a smoothbore shotgun, with the gunpowder mass adjusted for the desired velocity. The resulting fragments are collected (See Figure 2) and burned in a closed-bomb apparatus. When an undamaged cylinder of propellant is burned in a closed bomb, the pressure history in the bomb can be calculated from the separately-measured pressure-dependence of the linear burn velocity, the equation of state of the gas products, and an analytic form factor that describes the changing surface area of a cylinder burning from the outside in. When the collected fragments are burned, the pressure rise is faster due to the increased surface area. The test is usually not analyzed to determine the surface area. Instead it is standardized. For a standard-mass sample in a standard-volume closed-bomb vessel, the impact velocity causing a specific value of the maximum pressurization rate is recorded as the critical impact velocity

(CIV). Large values of CIV are associated with materials that are mechanically robust – a high velocity is required to break the propellant into small pieces.

Occasionally large solid rocket motors experience launch failures or launch aborts. If that happens before the rocket has traveled far from the launch pad, the fallback of the motor, whether on land or sea, can cause an explosion. If the motor is large enough, the explosion will produce air blast that can damage people or facilities some distance from the launch area. During our study of the consequences of fallbacks, we developed a model (Propellant Energetic Response to Mechanical Stimulus, PERMS) [3] that described the creation of surface area as a result of mechanical insult for a solid rocket propellant based on shotgun test results. The composition is typical for US Transportation Class 1.3 propellants – 12% Hydroxy-terminated polybutadiene (HTPB) binder, 30 % Aluminum powder (30 μm spheres), and bimodal Ammonium Perchlorate. Computer simulations of the impact, using a strength description taken from split Hopkinson bar compression tests, led to the typical distribution of plastic strains throughout the volume that is more intense near the impact face [2]. At one specific velocity, the photograph of the rubble pile included a piece from the rear of the projectile that was (apparently) undamaged. (See Figure 2b) Comparison with our simulations showed that part of the cylinder had experienced a plastic strain less than 10%. We found that describing surface to volume ratio (S/V) as a linear function of plastic strain with a lower cut-off value of 10% led to computed burn-rates that gave computed pressure histories consistent with the measured pressure histories over the range of impact velocities tested. With slight changes to the parameter values, we could also achieve comparable agreement for tests of other, similar propellants.

2.1.1 Calibration for UK HE by fragment observation

We applied the PERMS model to describe damage to the UK explosive we are studying. The model functional form and parameter values are,

$$\frac{S}{V} = 80(\varepsilon_p - 0.2) \text{ cm}^{-1},$$

where ε_p is the plastic strain. For a specific simple strength description, Y = 22 MPa, we calculated the plastic strain and S/V that resulted from a test similar to the UK variant of the Steven test [4, 5], but without a cover plate. Illustrations of various low-speed impact test geometries are shown in Figure 3. Photographs of the collected rubble were compared with results for the model with various parameter values for this test and also for spigot tests [6]. The comparison is necessarily qualitative, since the fragment size distribution was not measured using either sieve analysis or closed bomb burning. The qualitative result for the modified Steven test (Figure 4) is satisfactory. In that figure, a few pieces with a triangular cross-section are visible. That cross-sectional shape corresponds to the undamaged volume located in our simulation at the outer periphery of the sample, adjacent to the Teflon ring. The computed S/V is represented in Figure 4 by a collection of spheres with the calculated S/V distribution. The spheres, with a smooth surface, are necessarily smaller than fragments with a rough surface but the same surface area.

2.1.2 Calibration for UK HE by air blast measurements

For our study of rocket motor fallbacks, we calculated the efficiency of creating air blast from energy sources in which the energy release was extended in time, although not in space [7]. For that application the concern was blast damage in towns near the launch site, so the emphasis was on far-field blast, with peak pressure approximately 10 kPa, which is sufficient to damage windows. For that case, we found that if the energy were released in a time shorter than the positive phase duration of the air blast, the blast peak overpressure was the same as that resulting from a detonation. For a given peak overpressure, the positive phase duration of the blast wave is proportional to the cube root of the energy released.

In low-speed impact testing, the blast wave is measured at comparable peak overpressure to those we used in our study [7]. For a detonation of 6 grams of bare explosive measured at 2 meters, the peak overpressure is 11 kPa and the positive phase duration is 0.9 msec. We can estimate the size of the particle that burns 90% of its mass in a time equal to the positive phase duration by knowing the (pressure-dependent) burn velocity. If we assume that the HEVR takes place at a pressure of 200 MPa, the burn velocity is about 200 mm/s. For a sphere 0.7 mm diameter, 90 % is consumed in the required time. For our purposes, we account for the partial burning of larger fragments by assuming that only the mass of particles smaller than 1 mm contributes to air blast and does so with 100% efficiency. None of the larger fragments contributes. With that assumption, we can calculate the peak pressure from that mass of uncased explosive at the experimental gauge locations, and also the peak pressure from the detonation of the entire uncased mass of explosive.

The surrounding casing is known to reduce the air blast efficiency by absorbing some of the explosive energy in fracture, deformation, and kinetic energy. For the bolted test vehicles used in low speed impact testing, however, venting occurs at a relatively early stage in the event. Once the casing has vented, the escaping gas products will contribute to the air blast. The relative reduction in blast for full and partial reaction was not measured, and is difficult to calculate or estimate. For now we have assumed that the reduction would be the same fraction. With this assumption, the ratio of peak overpressure for uncased charges will be the same as for the cased charges.

Using these approximations, the results of our calculated particle size distribution for the fines can be compared with experiment. (See Table 1) We plan to examine the effect of the surrounding structure on air blast in the future. However, a more direct approach is to measure the surface area that results from mechanical insult whether by particle size measurements or by burning. For the next series of low velocity impact tests performed by AWE, it is planned to photograph the recovered fragments so that shape-recognition software can be used to establish the particle size distribution.

2.1.3 Status of surface area model

We have calibrated the parameters of a surface area model developed for propellants by qualitative comparison of photographs of the rubble pile and also by qualitative comparisons of the air blast measurements with estimates of the air blast caused by the fines of the particle size distribution. At this point, the parameters given have at most one significant digit. More quantitative data are required for more quantitative calibration.

2.2 Strength model

The PERMS model for surface area development uses plastic strain as the independent variable. In the Taylor test (which is the essence of shotgun test) the kinetic energy of the projectile is absorbed by plastic work. As a result, the plastic strain distribution depends on the compressive flow strength of the projectile. As a first approximation, the average final plastic strain, ε_p, is given by

$$\varepsilon_p = \ln\left(\frac{L_f}{L_0}\right) \approx -\frac{\rho_0 U^2}{2Y}$$

where L_0, and L_f are the original and final projectile lengths, ρ_0 is the projectile density, U the impact velocity, and Y the compressive flow strength [2]. As a result, a damage model based on plastic strain must be recalibrated whenever the constitutive model for the projectile material is revised. It is possible that a damage model based on plastic work would be less sensitive to revisions to the constitutive model. The choice of plastic strain was driven by the consideration that the simulation program in which the PERMS model was originally embedded did not carry plastic work as a history variable.

As an intermediate step, we developed an expedient PRS (Pressure-, strain-Rate-, and strain- dependent) model that fits the available data [8], which include uniaxial compression tests at strain-rates from 10^{-5} to 3000 sec^{-1}, and also triaxial compression tests (with prescribed lateral pressure) at low strain-rate. The model also accounts for ambient temperature effects by a shift in the strain-rate, similar to the development of a master curve such as those used for polymers. The model has been tested for reasonableness of behavior in various hypothetical compression test geometries and also for one-dimensional shock propagation. The functional form of the model is

$$Y = Y_T\left(\dot{\varepsilon}_p\right) f_P(P) f_\varepsilon(\varepsilon_p),$$

where Y_T is the (ambient temperature-dependent) tabular fit to uniaxial compression testing as a function of strain-rate including split Hopkinson bar test results. The factor f_P is a tabular fit to the pressure dependence of the yield stress, scaled to have the value 1 for uniaxial compression. The factor f_ε is a work-hardening function of plastic strain, scaled to have the value 1 at zero plastic strain. Data for triaxial testing at high rates would be required to do a proper calibration, but at present such data do not exist for the UK explosive. The solution method follows that of Steinberg and Lund [9], although we have taken the independent variable to be the log of the strain rate. The use of a tabular form is a convenient way to fit experimental data, but the resulting discontinuities in slope require a robust solver. The model is presently being incorporated in the UK equation of state (EOS) package. We will be applying it to simulations of low-velocity tests soon.

2.3 Porosity model

In addition to creating surface area, the volume of the most damaged material must also have been given some porosity. If that were not the case then although cracks and fragments were created, there would be no open channels for the flame to enter. The

flame, once started, could not then propagate into the damaged material. Sustained shearing of high-density fragmented material, which is the way that the fragment size is reduced in our model, results in an increase in porosity (dilatancy) and a pressure and porosity dependent shear strength. Dilatancy, first described in the late 19th century [10], is the increase in volume that occurs when granular materials undergo shear strains at constant normal stress. The phenomenon is well understood in the mechanics of rocks and soils, for which models have been developed and used successfully. There is a characteristic volume strain in granular soils that depends on the normal stress, which is described in the soil mechanics literature as the limit state. Soils that start out under-dense get denser in shear. Soils that start out over-dense (the case for developing a fragmented material from initially intact solid) expand in shear. This volume increase is conceptually important for flames to spread in broken material.

Flow surfaces for geologic materials and concrete have been developed that exhibit many of these characteristics [11,12]. They develop a history variable related to porosity. That variable, in combination with the characteristic dimension from S/V, can be used to calculate permeability for flame spread. We plan to implement such a model, suitably modified for the observed strain-rate and ambient temperature dependence. Development of this coupled mechanical response model is a future task.

3. HE ignition

3.1 Calculated ignition criterion

Ignition is critical to analyzing whether a specific mechanical insult leads to HEVR. Some have used modified shock-to-detonation models for HEVR response [13]. Both simple energy flux criteria [14] and the more complex reactive flow models [15,16] for shock-to-detonation require a shock pressure to be sustained for some period of time. There are theoretical objections to this approach for HEVR and pragmatic ones as well. The main theoretical objection is that HEVR is generally not a detonation. Substantial quantities of unreacted explosive are found scattered about the test area even when a violent event is recorded on blast gauges. The steel confinement is in much larger pieces than is found after a deliberate detonation. In addition, the steel lacks the characteristic appearance that results when it has been adjacent to a detonation. The main pragmatic objection is that the pressure or compressive stress calculated at the HEVR threshold is substantially different for different test geometries.

Several different mechanical insults have been applied to the UK explosive [5,6] including US and UK variants of the Steven test, spigot tests with and without steel confinement, drops, and oblique impacts. The ignition limits of those tests are given in Table 2, together with the calculated maximum normal stress.

For an ignition model, we use the observation that in low-speed impacts, such as the Susan, Steven, skid, and UK spigot tests, ignition is accompanied by significant shear deformation. Without identifying whether the localization mechanism is crystal twinning, continuum shear bands, friction, or grain-to-grain interference, we use properties of the stress tensor to identify where shear deformation is occurring.

If the principal stress deviators are ordered algebraically, the ratio of the intermediate stress deviator, s_2, to the equivalent stress, Y, is zero in shear, +1/3 in uniaxial compression, and -1/3 in uniaxial tension (for stress considered positive in tension). A shear-weighting factor, f_τ, given by

$$f_\tau = \left(2 - \frac{3|s_2|}{Y}\right),$$

has the value 2 in shear and 1 in tension or compression. If that expression is raised to a small power, approximately 4, then there is an order of magnitude difference in the factor to weight plastic strain developed in shear compared to that developed in tension or compression. Alternatively, J_3, the third invariant of the stress deviator tensor, may be used. The value of J_3 is given by

$$J_3 = s_1 s_2 s_3 = \det\left[\mathbf{s_{ij}}\right]$$

where s_{123} are the principal stress deviators, and $\mathbf{s_{ij}}$ is the stress deviator tensor. The alternative weighting factor, f_τ', given by

$$f'_\tau = \left(2 - \frac{27|J_3|}{2Y^3}\right)$$

also changes between 1 for uniaxial compression or tension and 2 for shear. Although the values for intermediate states (Lode angles) between the extremes have somewhat different values for f_τ' and f_τ, the primed version would also work, and is more customary in the mechanics literature. Since the intermediate principal stress is also needed for the normal stress weighting term, the computational efforts expended for either weighting factor are probably about the same.

The ignition model also contains an extra weighting term for the normal stress acting on the plane of maximum shear. If that stress is tensile, the weight is zero. This weighting term is consistent with the observation that lighting a match is more efficient if you press the match to the rough surface while striking (introducing a shear deformation).

$$\mathrm{D}_{\mathrm{ignition}} = \int_0^t \left(2 - \frac{3|s_2|}{Y}\right)^5 \left(\frac{p + s_2/2}{50\mathrm{MPa}}\right)^{1/2} \dot{\varepsilon}_p dt,$$

Here we use the hydrocode convention that positive pressure and negative stress deviators are compressive. When the value of $\mathrm{D}_{\mathrm{ignition}}$ reaches 500, ignition occurs. The value of the ignition criterion is given in Table 3 for cases we calculated. The free parameters and the ignition value of 500 were chosen on the basis of these comparisons of experiment with simulations using a constant yield strength of 22 MPa.

The results of the simulations for the ignition limits in the LLNL Steven test (110 m/s) and the AWE spigot intrusion test (28 m/s) were consistent with the criterion. In both the Steven and long spigot tests, ignition is accompanied by pinch. By pinch, we mean that two metal parts, *e.g.* the spigot and the back plate, make contact by squeezing out explosive that was originally between them. Pinch is also observed to accompany ignition in the Susan test. There the explosive is extruded through fractures in the aluminum housing. We note in Figure 4 that there is evidence of pinch – the shiny circle of base plate material – that was not accompanied by ignition. In any event, pinch is a severe localization of shear strain accompanied by normal stress, which is the basis of our ignition model. However, the result of the short spigot test simulation, where pinch does not occur, was that the calculated ignition parameter was 250. The experiment at that velocity resulted in ignition. Simulations with finer resolution for the short spigot test at the ignition velocity gave an ignition parameter just about equal to 500. However, refining the mesh of the long spigot (with pinch) and the Steven test (with pinch) also doubled the value to 1000.

There is a fundamental issue with the simplified constitutive model we used for the simulations in which there is a large frictional resistance to sliding. The Eulerian simulations of the Steven and spigot intrusion tests are the limiting case of a large friction coefficient, by virtue of the single velocity for a mixed cell that is dominated by relatively high density steel. In gas dynamics simulations, the gas viscosity, together with the free-stream transverse velocity, provides a characteristic length that is the boundary layer. In our simulations with a constant shear stress, the computational boundary layer is one computational mesh (or so). As a result, increasing mesh refinement increases the shear strain near the boundary without limit. We anticipate that the rate and pressure dependent PRS model will alleviate some of the mesh sensitivity.

3.2 Contribution of friction to shear localization

A deceptively simple geometry to study the effects of friction on deformation is to use a disk specimen between two rigid plates, which is the nominal geometry of disk forging [17] and split Hopkinson pressure bar (SHPB) testing [18]. The advantage of the latter is that the test is performed at a nominal strain rate of 2000 sec^{-1}, which is similar to that experienced in the low-velocity insults we are studying. In normal SHPB testing, care is taken to reduce the fiction coefficient by the use of MoS_2 lubricants, and to reduce the ratio of diameter to thickness, *D/t* to minimize the effect on the measured stress. For a small friction coefficient, the average stress in the sample [17] is given by

$$p_a = Y\left(1 + \frac{\mu D}{3t}\right),$$

where Y is the (constant) flow stress, μ is the friction coefficient, D is the increasing disk diameter, and t is the decreasing disk thickness. In this low friction coefficient limit, the surface of the disk slips against the platen. For high values of the friction coefficient, more than 0.57, the entire surface sticks and deformation is by sub-surface shear localization. For intermediate values, some of the surface slips and some sticks. In accident scenarios and low-speed impact testing, little consideration is given to the measurement or control of friction, so that the friction coefficient is unlikely to be small. The effect of friction, then, is to increase the apparent resistance of the test sample to deformation, and also to introduce shear strain localization [19]. In our model, these two factors increase the development of damage and the likelihood of ignition.

Experimental measurements of dynamic deformation of ring specimens [20] show a significant scatter in the results, from which may be inferred a variation in the friction coefficient of order 50%. The significance of this for HEVR testing is that it is a potential cause of overlap between go and no-go test results. A limited number of measurements of the friction between explosives and other materials have been performed [21,22]. The nominal friction coefficients are fairly large, in the range of 0.3 to 0.5.

4. HE energetic response

4.1 Flame propagation

Before the porosity model is implemented, we will need an expedient model for flame propagation. In the interim, we will assume that sufficient porosity exists throughout the damaged volume to permit flame spreading, once the ignition criterion has been met somewhere in the computation. We will assume that the flame propagation speed is some fraction, about 0.3, of the sonic velocity of the hot gas products. If a given

computational element has been ignited, whether by mechanical means or flame propagation, we proceed to calculate the reaction rate.

4.2 Calculation of the reaction rate

Once ignition has been achieved, the mass rate of conversion from reactant to product for an assembly of fragments burning from the outside in is given by

$$\dot{m} = \rho S v ,$$

where m is the mass of gas (product) created, ρ is the density of the solid (reactant), S is the total surface area that is burning, and v is the propagation velocity of the flame normal to the local surface. The surface area decreases during the deflagration as the fragments get smaller. If the fragments are compact objects, then the changing surface area is given by

$$S = S_0 (1 - \lambda)^{2/3} ,$$

where S_0 is the surface area before burning begins [3], and λ is the extent (mass fraction) of reaction.

Measurements with the LLNL strand burner [23, 24], diamond anvil cell experiments, and our simulations of constant pressure flame propagation [25] report the velocity as that propagating into the compressed solid. Closed bomb tests on, for example gun propellants, are typically not corrected for the changing density during the test. The form factor used to account for the changing surface area when interpreting the measured pressure increase is based on the original, uncompressed geometry. Using the isotherm of the explosive reactant at room temperature as a guide, there is a 3% increase in the solid density at a pressure of 0.4 GPa. For gun propellants, where 0.4 GPa is at or near the maximum design pressure, ignoring the correction is appropriate. For our application, we will retain the correction in the event that considerably higher-pressure excursions may be observed.

The flame speed of several HMX-based explosives has been measured in the LLNL strand burner at pressures up to 0.6 GPa [26]. In general, the laminar burn speed has the simple form observed, at least in limited pressure ranges, for gun propellants, rocket propellants, and explosives:

$$v = v_0 \left(\frac{p}{p_0} \right)^n ,$$

where v_0 is the flame speed at the reference pressure, p_0. For HMX and RDX-based explosives, the exponent, n, is about 1. For HMX, the flame velocity at 1 GPa is 1 m/s. For RDX, it is 0.75 m/s.

In certain circumstances, both HMX and RDX-based explosives with low binder content exhibit a sudden increase in the apparent burn velocity [26] called deconsolidative burn. If the resulting time derivative of pressure (or mass-burning rate) is interpreted as being caused by an increase in surface area, then surfaces have been formed that correspond to fragments with diameters from 0.1 to a few mm. In general, the occurrence of this sudden increase does not seem to be correlated with pressure, but rather shows up after 20% or so of the strand has burned. It is rarely reported in closed-bomb tests of gun propellants [27]. If it happened to already-fragmented material, it would be reported as a smaller effective fragment size, and not separable from the starting fragment size distribution. Comparisons with the surface area inferred from those

tests and other measurements of surface area are not routinely reported. The importance to this work is that deconsolidative burn would be a way of incorporating more than just the fragmented material in an HEVR event. Originally unfragmented material near the boundary of the fragmented region could also contribute to creating product gas rapidly enough to affect one or more of the violence measures.

4.3 Equation of state of decomposition products

The Jones-Wilkins-Lee (JWL) equation of state for explosive decomposition products has been a popular choice in detonation science since its introduction [28]. It combines a simple form with good accuracy for representing the adiabatic expansion of the products from a steady Chapman-Jouget (CJ) detonation. The adiabats have the general form

$$P = Ae^{-RV} + Be^{-SV} + CV^{-(1+\omega)}$$

where A, B, R, S, and ω are parameters and V is the volume relative to the reference volume, $V = \rho_0/\rho$ where ρ is the density and ρ_0 the reference density. The parameter C is used to specify the adiabat that originates at the CJ detonation state.

For states removed from the CJ adiabat, a temperature- or internal energy density-dependent form with constant specific heat, c_v, is used:

$$P = Ae^{-RV} + Be^{-SV} + \omega c_v T / V \text{ , or}$$

$$P = A(1-\omega/RV)e^{-RV} + B(1-\omega/SV)e^{-SV} + \omega e\rho_0 / V$$

where T is temperature, and e is the specific internal energy density. The latter form is in common use in hydrocodes where temperature is not required to solve the conservation of mass, momentum, and energy. The former is used in reactive flow models to describe the build-up to detonation, enforcing pressure and temperature equilibrium in the reaction zone.

Our application is far-removed from the CJ adiabat. If we were to maintain the same equation of state form, the parameters would need to be refit. However, the constant specific heat for the products is especially bad for high temperature-low density states in the pressure range where we are interested. Instead, we use the thermochemical equilibrium code Cheetah [29,30] to develop complete equation of state tables for the equilibrium products of explosive decomposition. The pressure on isotherms as a function of density is shown in Figure 5. The version of Cheetah we used to create the table assumes the products are above the critical point, so that no effort is made to rectify the van der Waals loops for those isotherms below the critical point. We have rectified the lowest isotherm (250 K) shown. We do not, in fact, anticipate using these equations in situations when the gas temperature is cooled below ambient. It is generally sounder practice, however, to interpolate such tables rather than extrapolate off the edges. The internal energy density of the reactant, which is the enthalpy of formation at the standard state minus the product of the standard pressure and reactant volume at the standard state, is subtracted from all points of the energy surface, so that the energy density given is relative to the energy of the reactant in Figure 6. The specific heat is shown in Figure 7, which illustrates our statement that a constant specific heat is a poor approximation.

The Cheetah equation of state can be used to calculate detonation conditions of the explosive. For an initial density of 1.84 Mg/m^3, the calculated detonation velocity is 8.59 km/s, and the associated particle velocity is 2.13 km/s, which give a detonation

pressure of 34 GPa. The measured detonation velocity is 8.79 km/s at this density, and associated particle velocity 2.28 km/s, which correspond to a detonation pressure of 37 GPa. This level of inaccuracy is acceptable for our purposes.

4.4 Calculation of two-species equilibrium

Our picture of HEVR is an assembly of explosive fragments surrounded by hot gas products, with flames progressing inward from the reactant-product interfaces of many fragments simultaneously. With this picture in mind, the assumption of pressure equilibrium between reactants and products is a relatively good one. If the interior of the fragments are cool enough that the reactant still has some strength, the actual equilibrium condition is that the normal stress in the solid is equal to the surrounding gas pressure, assuming that the pressure fluctuations in the hot gas are slow enough that the interiors of the fragments are at stress equilibrium. This will differ from pressure equilibrium by terms of the order of the compressive yield strength. For our purpose, pressure equilibrium should be accurate enough. If the yield strength is an important correction, then the pressures are low, and the difference in reactant volume will have little effect on the gas pressure.

If the flame front is thin relative to the fragment size, then the assumption of thermal equilibrium is poor. Most of the reactant will be at ambient temperature, and so exhibit neither thermal expansion nor reduced stiffness. If the flame front is thick relative to the fragment size, then thermal equilibrium is a relatively good assumption, but the picture that a progressing flame separates products from reactants is poor. For that case, a better picture is the simultaneous evolution of chemical species throughout the fragment with the kinetic rates dependent on the local temperature. We have performed direct numerical simulations of the flame propagation speed and thickness as a function of pressure in the range 5 to 50 GPa [25] and more recently extended the calculations to pressures as low as 0.1 GPa [31]. These simulations do not include species diffusion. At the higher pressures, the approximation is a good one – species diffusion is inhibited relative to thermal diffusion because the high density of gas products makes species migration difficult. At lower pressure, however, the two diffusivities are approximately equal. As a result, the effective kinetic rate at low pressure is slowed by the reduction of species concentrations [32, 33], which will tend to slow the flame propagation speed and increase the flame thickness. In the pressure range of interest to HEVR, 0.1 to 5 GPa, we estimate that the flame thickness is of order 0.2 μm. We have also performed a few simulations for the case where two flame fronts are propagating inward from plane parallel surfaces. As the remaining unburned reactant is heated by conduction, the flame, now propagating into reactant with temperature increased above ambient, accelerates [34]. This will contribute to an effective speed-up in the mass-burning rate when the fragment size approaches the flame thickness.

We developed the method of isochoric burn [35] to calculate the equation of state for a mixture of reactant and product. The method uses pressure equilibration, but relied on a detailed simulation of flame propagation to partition the energy. From those simulations, we observed that for subsonic flame propagation, the reactant was compressed along its adiabat starting from its initial temperature. The energy density in the gas was more complicated. That portion of the gas products that evolved first was further compressed by the evolution of additional product. As a result, there was an

energy density gradient in our one-dimensional simulations that would be leveled out by multi-dimensional mixing. Implementation is a two-step process. The computational zone first equilibrates pressure to the new volume each computational step using the previous extent of reaction. For this step the energy is apportioned to both solid and gas by adiabatic compression. The extent of reaction is increased according to the local pressure and reaction extent. For this step, the reactant is again on its adiabat, but the gas energy density is adjusted to conserve energy. The extent of reaction, λ, is a parameter between the values of 0 and 1. For small values of λ ($< 10^{-6}$) the pressure and temperature are calculated as if there were no gas. For large values ($> 1 - 10^{-6}$) pressure and temperature are calculated as if there were no solid.

In general, starting at an arbitrary initial temperature and pressure, the energy density of the solid is not zero, as is assumed in the product equation of state table. This is accommodated in the energy conservation equation,

$$e = \lambda(e_g - e_{s0}) + (1 - \lambda)e_s,$$

where e is the internal energy of the computational zone, and e_g, e_s are the internal energy density of the gas (product) and solid (reactant). The value of e_{s0} is established from the initial condition of pressure and temperature for the solid.

5. Summary

5.1 Conceptual model

We have developed a conceptual description of HEVR from mechanical insult that differs from previous analyses, such as [13]. First in the sequence of events is the production of damage by the mechanical insult. For our purpose, damage is expressed as surface area, accompanied by enough open porosity to propagate flames. The damage is localized near the impact zones, and is increased as the power of the insult increases. Secondly, ignition happens in a region of that damaged zone that undergoes intense shear. The shear localization is enhanced by friction, and the likelihood of ignition is enhanced by compressive normal stress on the plane of maximum shear. Thirdly the flame propagates in the damage zone and ignites the surfaces that have been created there. The mass-burning rate, although driven by a flame speed that is very subsonic (on the order of 10 cm/s) can result in a rapid pressure rise as a result of large surface area. Finally, expansion of the surrounding structure reduces the driving pressure. If the expansion is rapid enough, the hot gas cools and flame propagation can no longer be sustained. The structural expansion contributes both directly and indirectly to various measures of violence.

5.2 Progress to date

We calibrated the model for surface area by qualitative comparison with experimental rubble collected after impacts that did not lead to ignition, and qualitatively calibrated the mass of fines to one specific violence measure (air blast). We calibrated the model for ignition based on shear strain, although the simple yield strength model we used led to an ignition assessment that is dependent on the computational mesh size. We developed the PRS constitutive model that is Pressure-, strain-Rate-, and Strain-dependent to help reduce the mesh sensitivity. We implemented the models as post-processor (non-interacting) models to enable the assessment of damage, ignition, and an

estimate of the mass of explosive that will produce a violent response in both AWE and LLNL simulation programs.

6. Future work

In the future, additional computational activities will be focused on refitting the damage and ignition models using the new PRS constitutive model. We will be implementing the models in interactive form in LLNL and AWE simulation programs. More work is needed to define the detailed way in which friction results in strain localization, and whether the method of [36] can be used for a granular composite material where the granularity is comparable to the structure of the friction-affected zone.

At the same time, new experiments and measurement techniques need to be designed and implemented to isolate individual features of the model, and to assess the functional form and parameter values separately. Such features include the surface area and porosity, flame spread in a porous bed, circumstances of expansion that extinguish the flame, and the circumstances under which deconsolidative burn occurs.

7. Acknowledgements

Many of the features of the model described here are based on our earlier work on propellant behavior in launch fallback accidents. I am grateful for the long and fruitful collaboration with Jon Maienschein, Ed Lee, and Al Nichols from LLNL, as well as other members of the multi-organizational team, that began with that project. It is also pleasure to acknowledge the fruitful collaboration with AWE staff that was made possible by my secondment from LLNL to AWE that began in October 2007. The LLNL program managers who have sponsored that secondment are Al Ross, Bruce Watkins, Ron Streit, and Larry Fried. AWE personnel who have been directly supportive of this effort include Hugh James and Nick Whitworth of the HE detonation modeling team, Andy Jones and Bob Hughes of the HE test team, and Andy Abbott, who chairs the task force on HEVR at AWE.

8. References

1. G.I. Taylor, *Proc. R. Soc. A* **194**, 349 (1948)
2. M.L. Wilkins and M. W. Guinan, "Impact of cylinders on a rigid boundary," *J. Appl. Phys.*, **44**, 1200-1206 (1973)
3.J. M. Maienschein, J. E. Reaugh, E. Lee, "Propellant Impact Risk Assessment Team Report: PERMS Model to describe Propellant Energetic Response to Mechanical Stimuli," UCRL-ID-130077, February 27, 1998.
4. S.K. Chidester, L.G. Green, C.G. Lee, "A frictional work predictive method for the initiation of solid high explosives from low pressure impacts," *Proceedings, 10th International Detonation Symposium*, ONR 33395-12, Boston, MA 1993, pp785-792
5. S. Wortley, A. Jones, M. Cartwright, J. Allum, "Low speed impact of pristine and aged solid high explosive," *Proceedings, 12th International Detonation Symposium*, San Diego, CA, August 2002.
6. A. Jones, A.J. Dale, C.T. Hughes, M. Cartwright, "Low velocity impacts on explosive assemblies," *Proceedings, 13th International Detonation Symposium*, Norfolk, VA, July 2006.

7. J.E. Reaugh, E.L. Lee, J.L. Maienschein, “The production of air blast from solid rocket motor fallbacks”, JANAAF combustion, 1997.
8. D.M. Williamson, C.R. Sivior, W.G. Proud, S.J.P. Palmer, R. Grovier, K. Ellis, P. Blackwell, C. Leppard, “Temperature-time response of a polymer bonded explosive in compression,” *Journal of Physics D – Applied Physics*, **41**, 8, Article 085404, April 21, 2008.
9. D.J. Steinberg, C.M. Lund, “A constitutive model for strain rates from 10^{-4} to 10^{6} s^{-1},” *Journal of Applied Physics*, **65**, 1989, p1528.
10. O. Reynolds, “On the dilatancy of media composed of rigid particles in contact. With experimental illustrations,” *Phil. Mag.*, **20**, 1865, p469.
11. O.Yu. Vorobiev, B.T. Liu, I.N. Lomov, T.H. Antoun, “Simulation of penetration into porous geologic media,” *Int. J. Impact Engineering*, **34**, (4), 2007 p721.
12. M.B. Rubin, O.Yu. Vorobiev, L.A. Glenn, “Mechanical and numerical modeling of a porous elastic-viscoplastic material with tensile failure,” *Int. J. Solids Structures*, **37**, 2000, p1841.
13. K.S. Vandersall, S.K. Chidester, J.W. Forbes, F. Garcia, D.W. Greenwood, L.L. Switzer, C.M. Tarver, “Experimental and modeling studies of crush, puncture and perforation scenarios in the Steven impact test,” *Proceedings, 12th International Detonation Symposium*, San Diego, CA, August 2002.
14. F.E. Walker, R.J. Wasley, “Critical energy for shock initiation of heterogeneous explosives,” *Explosivstoffe*, **17**, (1) 1969, p9.
15. E. L. Lee and C. Tarver, “Phenomenological model of shock initiation in heterogeneous explosives,” *Phys. Fluids*, **23**, (12) December 1980, p2362.
16. C.A. Handley, “The CREST reactive burn model,” *Proceedings, 13th International Detonation Symposium*, Norfolk, VA, July 2006.
17. W. Schroeder, D.A. Webster, “Press-forging thin sections: effect of friction, area, and thickness on pressures required,” *J. Appl. Mechanics – Transactions of the ASME*, **16**, (3), 1949, p289.
18. L.D. Bertholf, C.H. Karnes, “2-dimensional analysis of split Hopkinson pressure bar system,” *J. Mech. Phys. Sol*., **23**, (1), 1975, p1.
19. Z. Huang, M. Lucas, M.J. Adams, “Modelling wall boundary conditions in an elasto-viscoplastic material forming process,” *J. Mats. Process. Tech*., **107**, 2000, p267.
20. R.S. Hartley, T.J. Cloete, G.N. Nurick, “An experimental assessment of friction effects in the split Hopkinson pressure bar using the ring compression test,” *Int. J. Impact Engr*., **34**, 2007, p1705.
21. K.G. Hoge, “Friction and viscoelastic properties of highly filled polymers: Plastic bonded explosives,” UCRL-70588, LLNL , 1967.
22. D.M. Hoffman, J. Chandler, “Friction of LX-04,” UCRL-CONF-207538, LLNL, Oct 2004.
23. M. Constantino, D. Ornellas, “A hybrid closed bomb-strand burner for very high pressure burning rate measurements”, UCRL-94769, JANNAF combustion, NASA Langley, Hampton VA, October (1986)
24. J.E. Reaugh, J.L. Maienschein, J.B. Chandler, “Laminar burn rates of gun propellants measured in the high-pressure strand burner”, UCRL-JC-127556, JANNAF combustion, West Palm Beach FL, October (1997)

25. J.E. Reaugh, "Multi-scale computer simulations to study the reaction zone of solid explosives," *Proceedings, 13th International Detonation Symposium*, Norfolk, VA, July 2006.
26. J.L. Maienschein, J.F. Wardell, M.R. DeHaven, C.K. Black, "Deflagration of HMX-based explosives at high temperatures and pressures," *Propellants, Explosives, and Pyrotechnics*, **29**, (5), 2004, p287.
27. Jim Barnes, Veritay Technology, Inc., Susan Peters, NSWC Indian Head, and Alice Atwood, NSWC China Lake, private communications, April 2008.
28. E.L. Lee, H.C. Hornig, "Equation of state of detonation product gases," UCRL-70809, *12th International Symposium on Combustion*, Potier, France, 1968.
29. L.E. Fried, W.M. Howard, P.C. Souers, "EXP6: A new equation of state library for high-pressure thermochemistry," *Proceedings, 12th International Detonation Symposium*, San Diego, CA, August 2002.
30. S. Bastea, K. Glaesmann, and L.E. Fried, "Equations of state for high explosive detonation products with explicit polar and ionic species," *Proceedings, 13th International Detonation Symposium*, Norfolk, VA, July 2006.
31. Aaron Wemhoff, private communication, LLNL, May 2008.
32. D.A. Frank-Kamenetski, *Diffusion and Heat Transfer in Chemical Kinetics*, Plenum Press, 1969, translation editor John Appleton.
33. Ya.B. Zel'dovich, G.I. Barenblatt, "Theory of flame propagation," *Combustion and Flame*, **3**, 1959, p61.
34. J.E. Reaugh, "Grain-scale dynamics in explosives," UCRL-ID-150388, September, 2002.
35. J.E. Reaugh, E.L. Lee, "Isochoric burn, an internally consistent method for the reactant to product transformation in reactive flow," *Proceedings, 12th International Detonation Symposium*, San Diego, CA, August 2002.
36. R.E. Winter, G.J. Ball, P.T. Keightly, "Mechanisms of shock-induced dynamic friction," *J. Phys. D. Appl. Phys.,* **39**, 2006, p5043.

9. Tables

Table 1. Mass of the explosive contributing to air blast at 2 m from the test and the mass of fragments smaller than 1 mm (fines) calculated with the model.

Test type	HE mass, g	Calculated fines, g	Calculated pressure, kPa	Calculated % of detonation	Measured % of detonation
Short spigot	175	5.6	11	15	15
Long spigot	175	7.5	12	18	20
LLNL Steven	225	31.5	26	31	25

Table 2. Ignition limits for the explosive under mechanical load

Test type	Impactor mass, kg	Velocity, m/s	Calculated maximum stress, GPa
US Steven	1.2	110	1.4
UK Steven	1.3	60	
UK Steven (open)	1.3	>80	>0.5
4.3 mm spigot	2		
4 mm spigot	2		
13 mm spigot	2	28	0.63
25 mm spigot	2		
50 mm spigot	2250	4	0.63
Drop	2250		
Oblique drop	5		
Short spigot	2	42	0.2

Table 3. Calibrated ignition criterion

Test type	Velocity, m/s	Result	Calculated ignition criterion
US Steven	110	Ignition	500
US Steven	100	No go	490
13 mm spigot	28	Ignition	540
13 mm spigot	22	No go	370
UK Steven (no cover plate)	80	No go	310

10. Figures

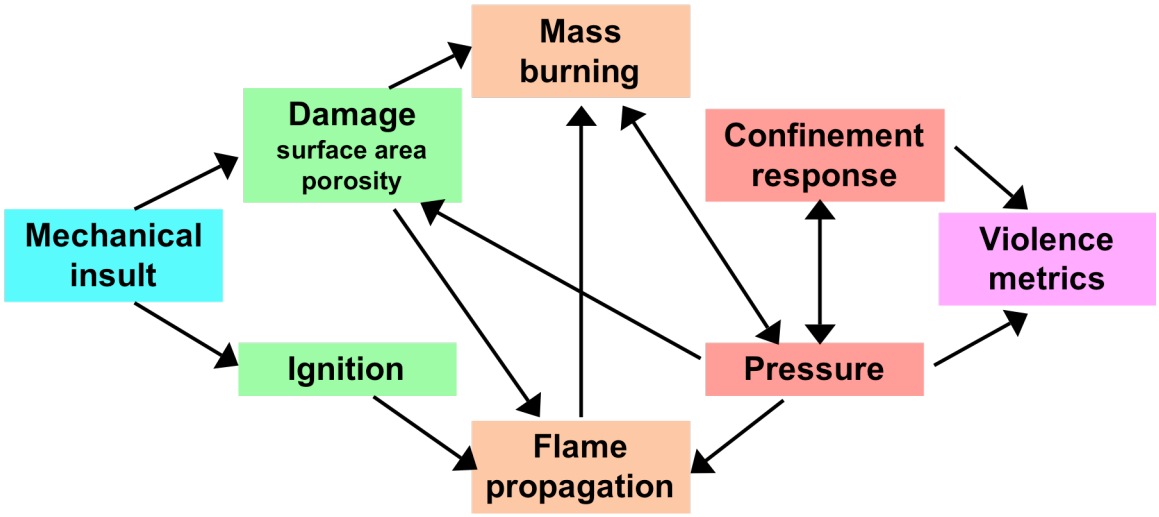

Figure 1. Interaction of the phenomena contributing to HEVR

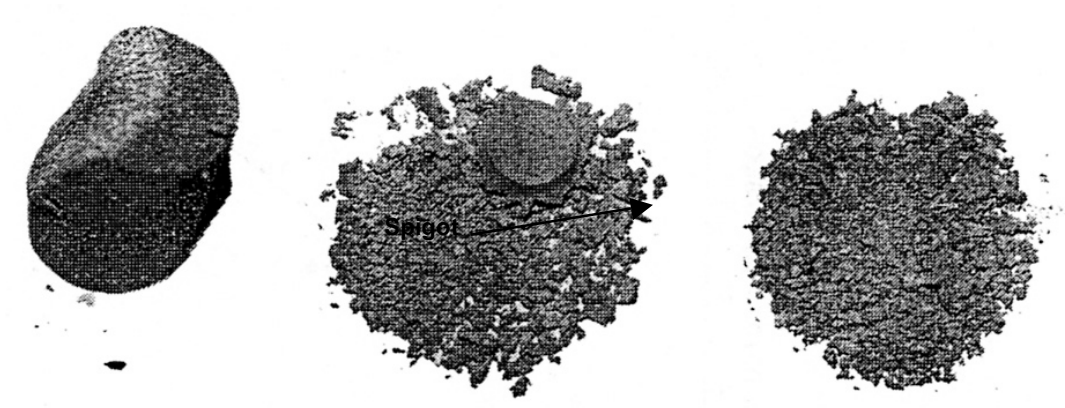

Figure 2. Residue from shotgun tests of Transportation class 1.3 propellant fired at 100, 170, and 230 m/s from left to right. The apparently intact rear of the projectile can be seen in the middle residue pile. (Photograph courtesy of Alice Atwood, NSWC China Lake)

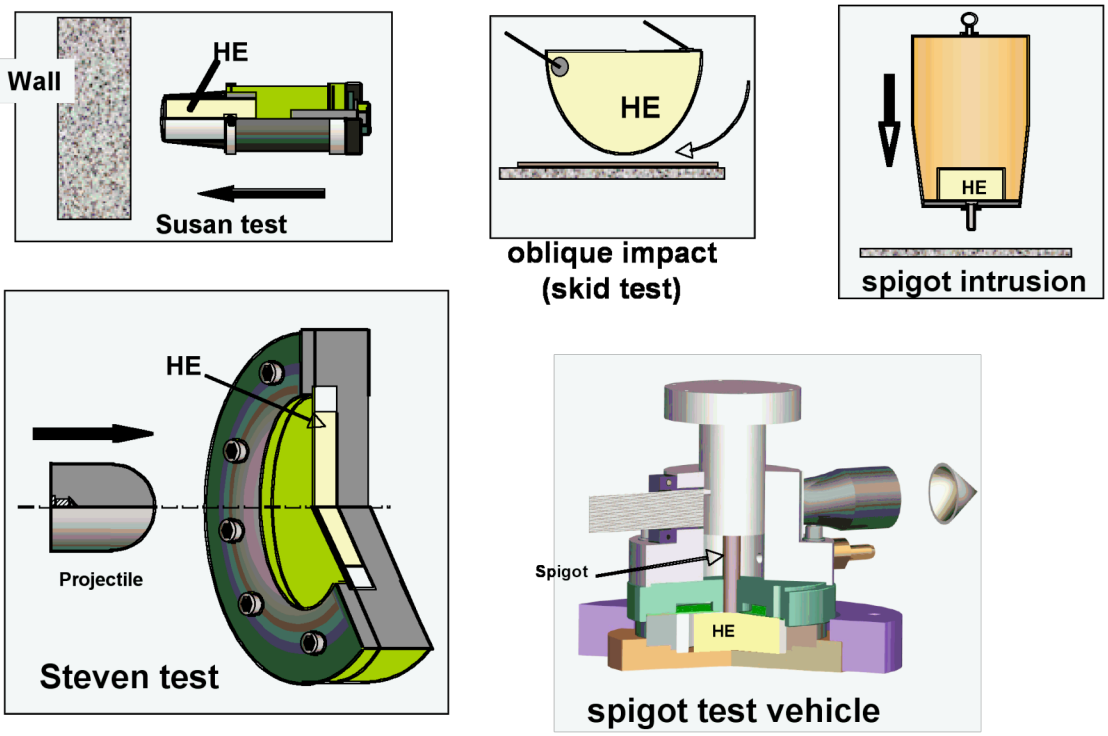

Figure 3. Illustration of various low-speed test geometries used for impact testing of explosives. Figures courtesy A. Jones, AWE.

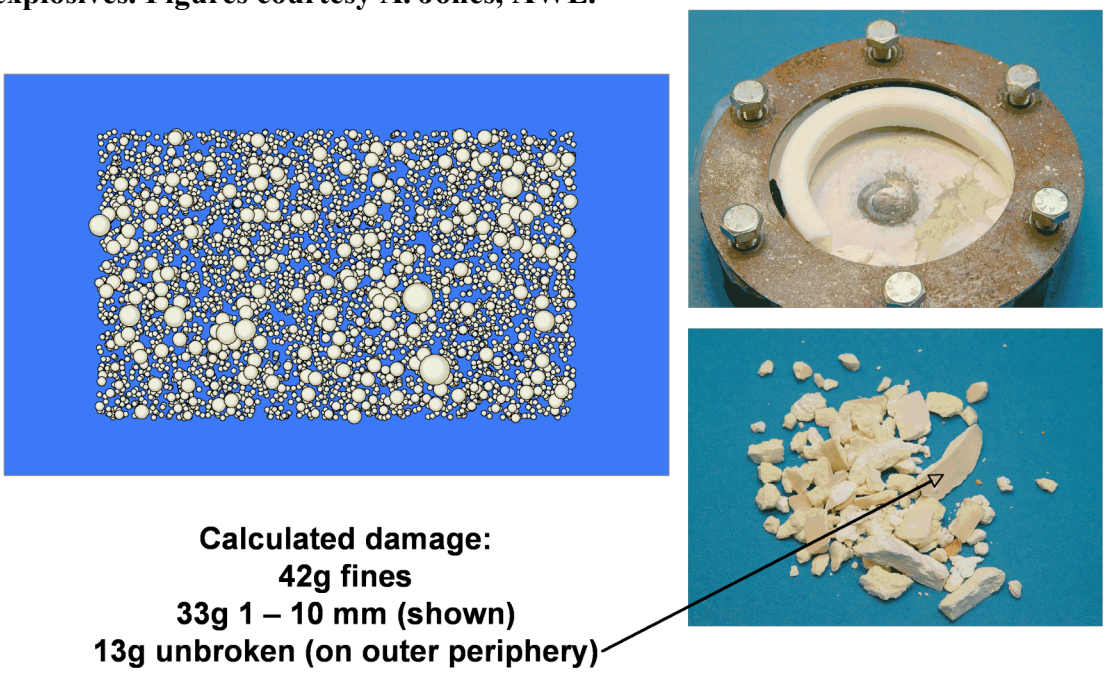

Figure 3. A UK Steven test (without the steel cover plate) at 80 m/s produced damage, but not ignition. The height of the Teflon ring (upper right) is 13 mm. The calculated result was that 13 g of unbroken material remained along the outer periphery with a triangular cross section. Residue from that location is also visible in the photograph of the experimental fragments. Photographs courtesy A. Jones, AWE.

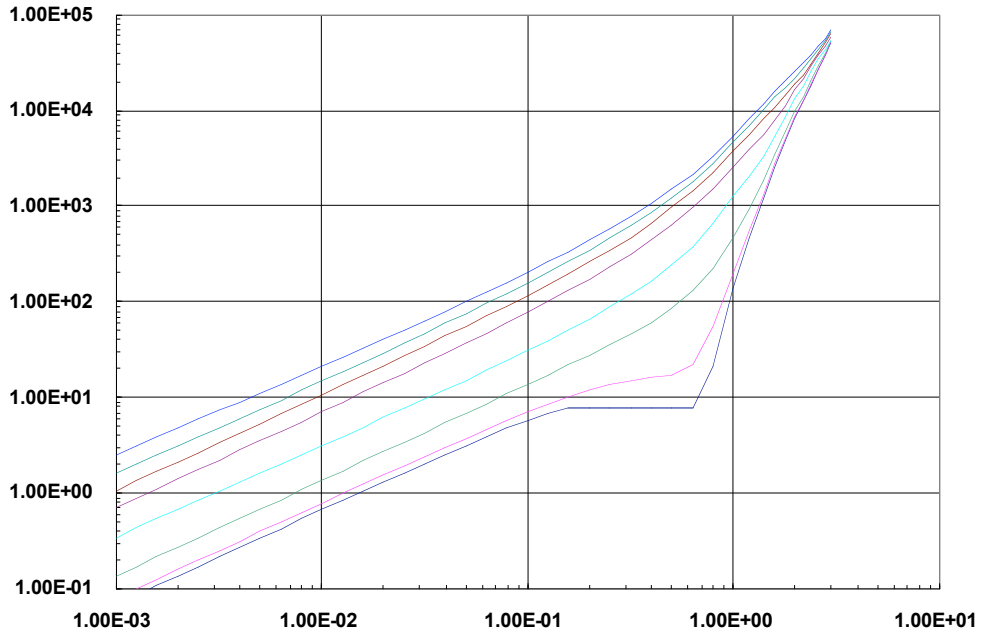

Figure 5. Pressure (MPa) as a function of density (Mg/m^3) on isotherms (from bottom to top) of 250, 298, 500, 1000, 2000, 3000, 4000, and 5000K.

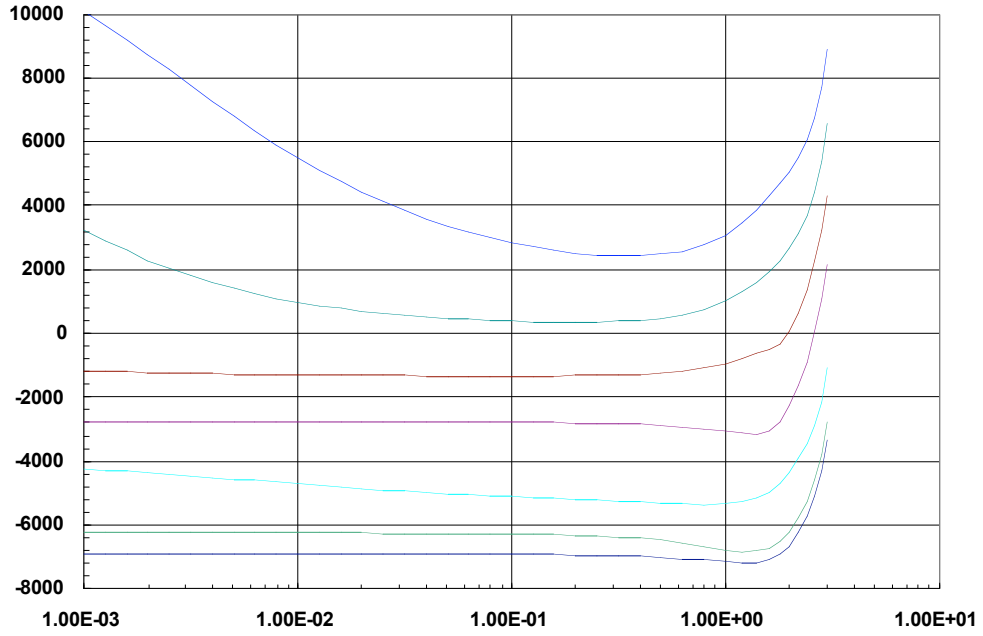

Figure 6. Internal energy density (J/g) as a function of density (Mg/m^3) on isotherms (from bottom to top) of 250, 500, 1000, 2000, 3000, 4000, and 5000 K. The 298 K isotherm is indistinguishable from the 250 K isotherm at this scale.

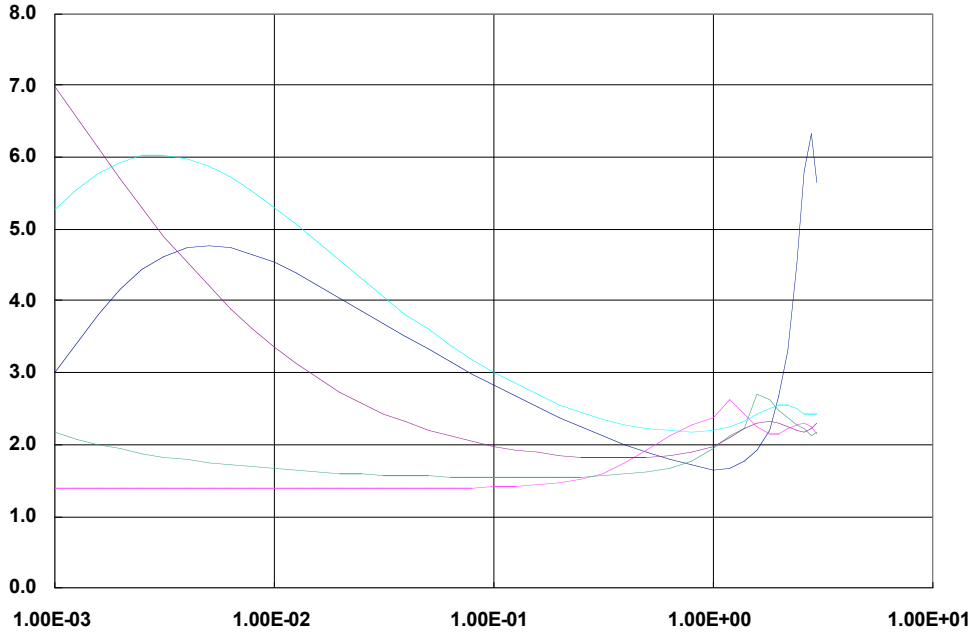

Figure 7. Specific heat at constant volume (J/g-K) as a function of density (Mg/m^3) on isotherms (from bottom to top at the lowest density) of 2000, 3000, 1000, 5000, and 4000 K. The non-monotonic behavior is the result of the changing equilibrium composition of the various product species on the isotherms.